GA–A27816

IDENTIFYING THE LOCATION OF THE OMP SEPARATRIX IN DIII-D USING POWER ACCOUNTING

by

P.C. STANGEBY, J.M. CANIK, D. ELDER, C.J. LASNIER, A.W. LEONARD, D. ELDON, M.A. MAKOWSKI, T.H. OSBORNE and J.G. WATKINS

AUGUST 2014

GENERAL ATOMICS

DISCLAIMER

GA–A27816

IDENTIFYING THE LOCATION OF THE OMP SEPARATRIX IN DIII-D USING POWER ACCOUNTING

by
P.C. STANGEBY, J.M. CANIK, D. ELDER, C.J. LASNIER, A.W. LEONARD, D. ELDON, M.A. MAKOWSKI, T.H. OSBORNE and J.G. WATKINS

This is a preprint of a paper to be submitted for publication in *Nuclear Fusion.*

Work supported in part by
the U.S. Department of Energy
under DE-FC02-04ER54698 and DE-FG02-04ER54761

GENERAL ATOMICS PROJECT 30200
AUGUST 2014

GENERAL ATOMICS

Abstract

In order to identify reliable scalings for the scrape-off layer (SOL) power width it is necessary to know the location of the separatrix in divertor tokamaks as accurately as possible, specifically its location at the outside midplane, omp, the standard reference location. Two methods are described which use power accounting to improve the accuracy of identifying the location of the omp separatrix. The first uses the infrared-measured deposited power profile at the outer target as the primary input, the "$P_{SOL}^{exhaust}$ Method". The second uses the measured power input to the SOL, obtained by subtracting the power radiated from inside the separatrix from the total heating power, the "P_{SOL}^{input} Method". These two power accounting methods are illustrated with the examples of 21 H-mode DIII-D discharges. High spatial resolution Thomson scattering measured profiles of n_e and T_e for the main SOL near the omp are also used as primary input to the analysis; only between-edge localized mode data are used here. The Thomson profiles are used to calculate the electron parallel conducted heat flux profiles which are then matched to the measured $P_{SOL}^{exhaust}$ and P_{SOL}^{input} by adjusting the location of the omp separatrix relative to that of the Thomson data. For these attached discharges, it is found that the values of R_{sep}^{omp} given by the two power accounting methods agree to within ~ 1 mm of each other and also to within ~ 1 mm of the values given by the "standard DIII-D method" described by Porter et al [Phys. Plasmas **5** (1998) 1410]. The shifted R_{sep}^{omp} results in only modest changes to the values of n_e and T_e at the omp separatrix relative to the "standard" values, increasing n_e^{sep} by ~ 10% and T_e^{sep} by ~ 20%.

PACS Numbers: 52.55.Dy, 52.55.Fa52.55.Rk

1. Introduction

In order to identify reliable scalings for the scrape-off layer (SOL) power width, it is necessary to know the location of the separatrix in divertor tokamaks as accurately as possible, specifically its location at the outside midplane, omp, which is the standard reference location for the SOL. In this paper, two methods are described which use power accounting to improve the accuracy of identifying the location of the omp separatrix. The first uses the infrared-measured deposited power profile at the outer target as the primary input; we will call this the "$P_{SOL}^{exhaust}$ Method". The second uses the measured power input to the SOL, obtained by subtracting the power radiated from inside the separatrix from the total heating power; we will call this the "P_{SOL}^{input} Method". The Thomson profiles are used to calculate the electron parallel conducted heat flux profiles which are then matched to the measured $P_{SOL}^{exhaust}$ and P_{SOL}^{input} by adjusting the location of the omp separatrix relative to that of the Thomson data. These two power accounting methods are illustrated with the examples of 21 DIII-D attached discharges from a current scan set and a power scan set. In a companion paper [1] these methods are compared with a number of other methods for identifying the location of the omp separatrix.

These power accounting methods are also applied here to *purely calculated* data obtained using the SOLPS edge fluid code [2] for the Fusion Development Facility (FDF) tokamak [3]. In this situation the location of the separatrix is known exactly, of course, and this therefore provides a test and calibration of the two methods.

In Sec. 2, the Thomson data are presented and the "standard" method that has been used on DIII-D for some time to identify the omp separatrix is decribed. In Sec. 3, the expressions are given for kinetically-corrected (flux-limited) electron Spitzer parallel heat conduction and profiles of $q_{\parallel e}^{kcSp}\left(R-R_{sep}\right)$ are calculated from the Thomson profiles. Section 4 describes the measured (by infrared thermography) power deposition widths at

the outer target and compares these widths with the ones theoretically expected for kinetically-corrected electron Spitzer parallel heat conduction, finding excellent agreement. Section 5(a) describes the $P_{SOL}^{exhaust}$ method and applies it to the DIII-D shots while in Sec. 5(b), this method is applied to SOLPS code-calculated cases in order to test and calibrate the method. Sections 6(a) and 6(b) do similarly for the P_{SOL}^{input} method. Section 7 compares the values obtained for R_{sep} by the two methods, finding that they agree with each other to within ~ 1 mm. Section 8 provides a sensitivity analysis, while Sec. 9 covers discussion and conclusions.

2. The DIII-D Thomson Data and the "Standard" DIII-D Method of Identifying the Location of the OMP Separatrix

The electron density and temperature are measured on DIII-D with a Thomson scattering system that views the plasma along a vertical line at a major radius of R = 1.94 m [4]. Recently, this Thomson scattering diagnostic has been upgraded [5]. Spatial and temporal resolution, as well as signal to noise ratio, have all been specifically enhanced in the edge region. This region is now diagnosed by 20 view chords with a spacing of 6 mm and a scattering length of just under 5 mm sampled at a nominal rate of 250 Hz. When mapped to the outboard midplane, this corresponds to ~ 3 mm spacing.

Examples of profiles, $T_e(R-R_{sep}^{standard})$ and $n_e(R-R_{sep}^{standard})$, for the 1 MA discharge 144977 are given in Fig. 1. All of the discharges used in this study are H-mode shots; only between-edge localized modes (ELMs) data have been used here.

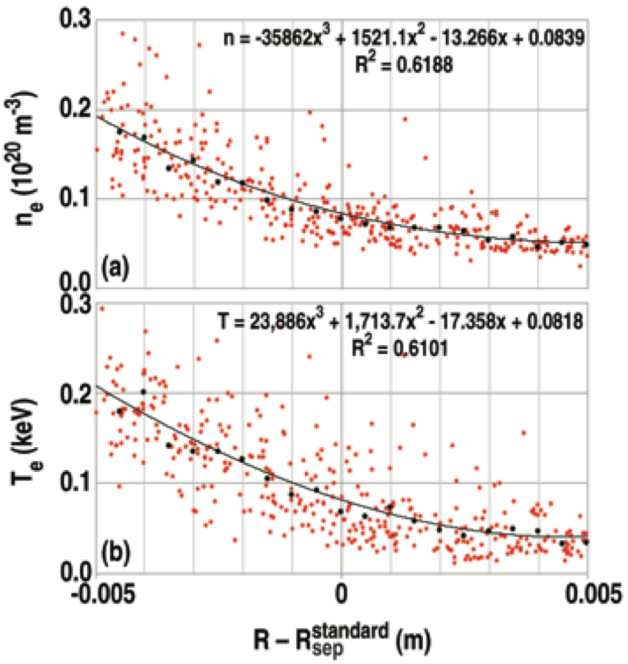

Fig. 1. Thomson scattering profiles for DIII-D discharge 144977. Cubic fits to all the TS data points (small symbols) within $x \equiv R - R_{sep}^{standard} \in [-5,5]$ mm are shown as solid lines. Also shown are values averaged over 0.5 mm intervals (large symbols). From cubic fits: $T_e(0)$ = 81.8/82.5 eV, $n_e(0)$ = 8.39/ 8.44x10^{18} m^{-3}, $\lambda_{T_e}(0)$ = 4.71/4.70 mm, $\lambda_{n_e}(0)$ = 6.32/6.50 mm; 1st value: for all TS points; 2nd value: for 0.5 mm-averaged points.

The values of $R_{sep}^{standard}$ are generated by a procedure which has been in use at DIII-D for the past ~ 15 years for assigning the value of the separatrix at the omp. This "standard DIII-D" procedure uses EFIT magnetic reconstruction and

fitting the Thomson profiles by hyperbolic tangent functions, then assigns the location of the separatrix $R_{sep}^{standard}$ according to a procedure described by Porter, et al [6]. This standard procedure is briefly as follows:

Best fits are made to the Thomson n_e and T_e data assuming a hyperbolic functional form:

$$Y(Z) = A_0 - A_1 \tanh\left[\frac{Z - A_2}{A_3}\right] = A_0 - A_1 \tanh[\xi], \qquad \xi \equiv \left[\frac{Z - A_2}{A_3}\right] \tag{1}$$

where the primary data are functions of the vertical coordinate Z which is the direction of the line-of-sight of the Thomson laser. Thus, four fitting parameters are generated for each of n_e and T_e (there is an additional Heaviside function included for fitting the data further inside the separatrix [6], but that is not relevant here and has been omitted).

On the basis of UEDGE code runs for a number of DIII-D cases, Porter, et al, concluded that the correct location of the separatrix is at $\xi_{T_e} = 0.5$, i.e. at:

$$Z_{sep} = A_2^{T_e} + 0.5A^{T_e}_3 \ . \tag{2}$$

That is, the separatrix is placed outside the location where the T_e-gradient is shortest, which occurs at $\xi_{T_e} = 0$, i.e. at $Z = A_2^{T_e}$, by a distance of half a normalized width, i.e. 0.5A $^{T_e}_3$.

The data and fit-function are then mapped to the omp using the EFIT magnetic reconstructed configuration, thus giving the value of $R_{sep}^{standard}$.

As noted by Porter, et al, there are a number of assumptions made in this standard procedure which are open to question, including:

1. The assumption of a hyperbolic fitting function lacks a fundamental basis and is arbitrary.
2. The various physics assumptions in the UEDGE code which may not be justified.

The primary objective of the present study is to see if the application of power accounting supports the reliability of the standard DIII-D procedure for identifying the location of the omp separatrix, or can suggest a better one.

As noted, the value of R is the major radius location of the Thompson data point mapped to the omp; it is calculated from (i) the measured (R, Z) location of the Thomson measurement, which is near but not at the omp, and (ii) mapping along the poloidal flux surface, as given by EFIT magnetic reconstruction, from the Thomson location to the omp. The Thomson data are for different times in the essentially constant part of the discharge; since the location of the separatrix is not exactly constant during the discharge, an EFIT calculation is made for the specific time of each Thomson measurement. There is error/uncertainty in the (R, Z) location of the Thomson diagnostic system and/or in the value for $R_{\rm sep}^{\rm standard}$. We are primarily interested in knowing accurate values of $T_{\rm e}(0)$, $n_{\rm e}(0)$, $\lambda_{T_e}(0)$ and $\lambda_{n_e}(0)$, i.e. the values at the omp separatrix, rather than their values at an absolute location in space, e.g. in machine coordinates (R, Z). In applying the power accounting methods, we can adopt one or other of the following assumptions:

(i) We can assume that the correct separatrix location in machine coordinates, $R_{\rm sep}^{\rm correct}$, is given by $R_{\rm sep}^{\rm standard}$ and that, in order to satisfy power accounting, the Thomson profiles (may) have to be shifted relative to $R_{\rm sep}^{\rm correct} = R_{\rm sep}^{\rm standard}$.

(ii) We can assume that the R-values of the Thomson data points are at the correct locations in machine coordinates and that, in order to satisfy power accounting, the value of $R_{sep}^{correct}$ (may) have to be shifted relative to $R_{sep}^{standard}$.

Although there is no fundamental justification for choosing (i) versus (ii) (nor some intermediate assumption), for specificity and clarity, we will assume (ii) here, i.e. we seek to find values of the correct separatrix location $R_{sep}^{correct}$ which will generally differ from $R_{sep}^{standard}$.

The main properties of the shots used in this study are given in Table 1, which also contains information on the statistics of the cubic fits to the Thomson data.

In Table, 1 the value of ΔR_{sep}^{std} is the amount that the major radius R-value of the omp separatrix was changed relative to the EFIT value by applying the "standard DIII-D procedure" described above (all data used here, e.g. in Fig. 1, have already had this shift applied; the shifts calculated below are therefore *additional* shifts). For example, for discharge 144977 ΔR_{sep}^{std} = -2.56 mm, so the omp separatrix was shifted *inwards*, which results in *increased* values of $T_e(0)$ and $n_e(0)$. To avoid potential confusion, it should be noted that some DIII-D scientists use the opposite convention to that adopted here, namely they take the omp separatrix location to be fixed and quote values for ΔR_{TS}^{std}, i.e. the shift to the Thomson profiles (as mapped to the omp), where $\Delta R_{TS}^{std} \equiv -\Delta R_{sep}^{std}$.

The choice of cubic fits is arbitrary; however, the effect of using other fits, e.g. quadratic ones, is small, see Table 2.

As shown in Table 1 there are a large number of data points for each shot, ~ 100-500. Are there enough for well-defined profiles? An indication is provided by discarding every second data point and considering the effect on the principal profile parameters, see Table 3. There are clearly more than enough data points.

Table 1

The 7th column gives the number of Thomson data points in the interval $R - R_{sep}^{standard}$ = -5 mm to +5 mm. The 8th and 9th columns give the R^2 values for the cubic fits to the Thomson data. The R^2 values for shots 144986, 7 are very low and these discharges are not be used in some of the tabulations, below. P_{heat}^{*}: * indicates ECRH, otherwise neutral beam heating. The value of $\bar{n}_e$ is the average of the highest and lowest value during the so-called "flat top" portion of the discharges used to collect Thomson data, e.g. 2.03–4.48 s for 144977; the variation is due primarily to the ELMs, but there is also some slower drift.

Shot	$\bar{n}_e$ (10^{20} m^3)	I_p (MA)	δ_u	P_{heat} (MW)	ΔR_{sep}^{std} (mm)	No. of Thomson data points	$R^2_{n_e}$	$R^2_{T_e}$
144977	0.56 ± 16%	1.00	0.25	2.64	-2.56	365	0.62	0.61
144981	0.78 ± 20%	1.48	0.20	2.59	-2.29	654	0.81	0.76
144982	0.79 ± 14%	1.48	0.20	2.83	-2.27	590	0.84	0.79
144986	0.24 ± 15%	0.52	0.23	2.25	-2.44	449	0.19	0.18
144987	0.22 ± 18%	0.52	0.23	2.24	0.54	299	0.09	0.15
144990	0.42 ± 19%	1.00		2.84*	-3.72	440	0.36	0.51
144992	0.44± 15%	1.00		2.84*	-3.88	389	0.58	0.65
144993	0.44 ± 16%	1.00	0.19	3.40*	-3.61	481	0.51	0.60
144994	0.63 ± 13%	1.48	0.14	3.33*	-2.50	202	0.65	0.63
145001	0.30 ± 13%	0.71	0.18	2.45*	-3.73	458	0.48	0.55
145002	0.30 ± 13%	0.72	0.19	2.56*	-4.65	430	0.45	0.47
148980	0.41 ± 9%	1.00	0.25	3.88	-2.92	149	0.74	0.74
148981	0.46 ± 7%	1.00	0.25	3.68	-3.40	131	0.57	0.61
148982	0.39 ± 10%	1.00	0.25	5.57	-1.80	313	0.54	0.54
148983	0.41 ± 10%	1.00	0.26	6.74	1.52	225	0.53	0.56
148984	0.40 ± 9%	1.00	0.26	7.09	0.58	141	0.62	0.64
148985	0.39 ± 9%	1.00	0.25	8.09	-0.96	200	0.40	0.41
148986	0.40 ± 9%	1.00	0.25	8.44	0.52	67	0.54	0.65
148988	0.53 ± 6%	1.00	0.38	4.12	1.27	180	0.51	0.53
148989	0.33 ± 10%	0.99	0.11	4.17	-2.95	262	0.68	0.59
148990	0.36 ±7%	0.99	0.12	3.95	-3.22	217	0.70	0.68
				Avg.	-2.02			

Table 2

The effect on the separatrix values of using quadratic rather than cubic fits is small. $\ell_{T_e}^{sep} \equiv \left[T_e / \left(dT_e / dR\right)\right]_{R=R_{sep}^{std}}$.

	T_e^{sep}	$\ell_{T_e}^{sep}$	n_e^{sep}	$\ell_{n_e}^{sep}$
Average ratio of quadratic fit value to cubic fit value	1.00	0.98	1.000	0.93
Standard deviation	0.004	0.14	0.003	0.11

Table 3

The effect of discarding every second data point on the values of the principal profile parameters extracted from the cubic fits.

	T_e^{sep}	ℓ_{T}^{sep}	n_e^{sep}	ℓ_{n}^{sep}
Average ratio of value using half the data points to all the points	1.00	1.02	0.99	1.03
Standard deviation	0.04	0.13	0.03	0.17

Further insight on the sufficiency of the number of Thomson data points is given in Fig. 2, which shows the effect on the values of the principal profile parameters for shot 144977 of reducing the number of data points used in the cubic fits from the full set of points, 365, in steps down to seven. As can be seen, there is not much effect until the number of data points is reduced below ~ 100.

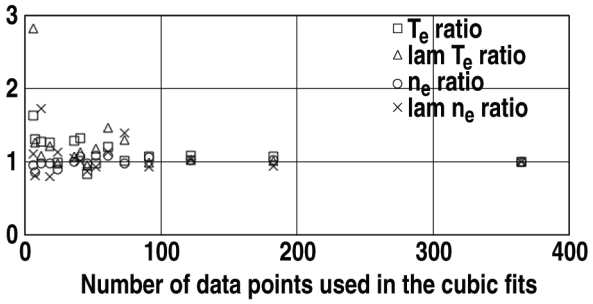

Fig. 2. For shot 144977, the effect on the values of the profile parameters of using less than all of the available Thomson data points. The vertical axis is the ratio of the extracted value normalized to the value extracted when using all the available data points (365) in the cubic fits: T_e ratio (squares), λ_{T_e} ratio (triangles), n_e ratio (circles), λ_{n_e} ratio (crosses).

3. Modelling the Electron Parallel Power Flux Density in the SOL Near the OMP

Near the separatrix and not too near the targets, parallel power transport in the scrape-off layer is typically dominated by electron heat conduction, rather than by electron heat convection or ion heat transport (Chapter 4 of Ref. 7). For sufficiently collisional electrons, the heat conduction is given by the Spitzer expression. The SOL is often only weakly collisional in the main part of the SOL, near the omp. In order to deal with this, models and codes for the SOL, such as UEDGE, SOLPS, etc., generally use a *kinetically-corrected-Spitzer* expression for the electron conducted power based on an expression for *flux-limited-conduction*. This is discussed in more detail in Sec. 26.2 of Ref. 7.

The cubic fits to the Thomson profiles for $T_e(R-R_{sep}^{std})$ and $n_e(R-R_{sep}^{std})$ were used to calculate (i) the Spitzer, (ii) the flux-limited and (iii) the kinetically-corrected-Spitzer, electron parallel power flux density profiles $q_{\|e}^{Sp}(R-R_{sep}^{std})$, $q_{\|e}^{fl}(R-R_{sep}^{std})$ and $q_{\|e}^{kcSp}(R-R_{sep}^{std})$:

$$q_{\|e}^{Sp}(R-R_{sep}^{std}) = -\kappa_{0e}T_e^{5/2}\frac{dT_e}{ds_\|} \approx 2\kappa_{0e}T_e^{7/2}/7L_{conn} \quad (3)$$

with q [W/m^2], T_e [eV]. L_{conn} [m] is the connection length for the outer SOL (Sec. 4.10 of Ref. 7), values are listed in Table 2. SOLPS uses the 21-moment expression [8] for the electron heat conduction coefficient κ_{0e}, which is also used here:

$$\kappa_{0e} = \frac{2.16\times 25000}{\ln\Lambda\left(1+0.27Z_{eff}\right)} \quad (4)$$

$\ln\Lambda$ is the Spitzer log factor. Some impurity level in the outer SOL plasma is assumed here, $Z_{eff} \sim 1.3$ (not measured).

(b) $q_{\|e}^{fl}(R-R_{sep}^{std}) = \alpha_e n_e\sqrt{eT_e/m_e}eT_e$. (5)

See Sec. 26.2 of Ref. 7, where q [W/m^2], T_e [eV], n_e [m^{-3}], e = 1.6x10^{-19} C, m_e = 9.1x10^{-31} kg, and α_e is the flux-limit constant [dimensionless] typically $\alpha_e \sim 0.3$ is used [2] and this value will be assumed here.

(c) $$1/q_{\|e}^{kcSp} \equiv 1/q_{\|e}^{Sp} + 1/q_{\|e}^{fl} \quad . \tag{6}$$

See Sec. 26.2 of Ref. 7.

In the present analysis, we will generally use $q_{\|e}^{kcSp}$. At least *mathematically*, $q_{\|e}^{Sp}$ and $q_{\|e}^{fl}$ represent the two limits of $q_{\|e}^{kcSp}$ and it is therefore potentially informative to consider what happens if either of these limits is assumed instead of $q_{\|e}^{kcSp}$; however, it is not clear that $q_{\|e}^{fl}$ represents a *physically* valid limit to the actual $q_{\|e}$ for very weak collisionality since the value of α_e was derived in the first place by assuming equation (6) and adjusting α_e to get agreement with full kinetic analysis of simple cases (Sec. 26.2 of Ref. 7).

An example of these parallel electron power flux densities are shown in Fig. 3, which is for shot 144977. The $q_{\|}$ values were calculated at 0.1 mm intervals using the cubic fits to the Thomson n_e and T_e profiles. Best-fit exponentials were then calculated for the $q_{\|}$ profiles for the interval $R - R_{sep}^{standard}$ = -2 mm to +2 mm.

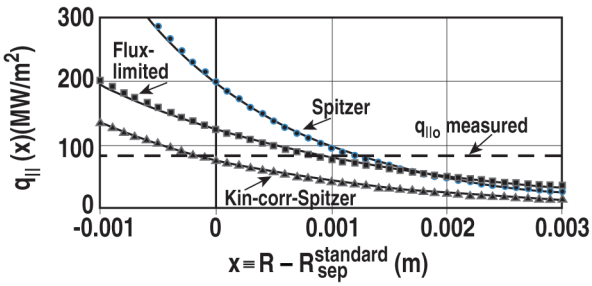

Fig. 3. For shot 144977. The $q_{\|}$ values (solid points) were calculated at 0.1 mm intervals using the cubic fits to the Thomson n_e and T_e profiles. Best-fit exponentials (solid lines) were then calculated for the $q_{\|}$ profiles for the interval $x \equiv R - R_{sep}^{standard}$ = -0.002 m to +0.002 m: $q_{\|e}^{Sp}=198e^{-697x}$ (circles), $q_{\|e}^{fl}=125e^{-443x}$ (squares) and $q_{\|e}^{kcSp}=76.3e^{-557x}$ (triangles). The dashed horizontal line is the value of $q_{\|0}$ obtained from the measured power deposition at the target and is discussed in Sec. 5.

We thus have convenient approximations of the form:

$$q_{\|e}^{X}(R - R_{sep}^{std}) = q_{\|0}^{X}(0)\exp[-(R - R_{sep}^{std})/\lambda_q^X] \quad (7)$$

where X stands for Spitzer, flux-limited or kinetically-corrected-Spitzer. For the example in Fig. 3, shot 144977, we have:

$q_{\|e}^{Sp}(0)$ = 198 (MW/m^2) and λ_q^{Sp} = 1/696.7 (m) = 1.44 (mm)

$q_{\|e}^{fl}(0)$ = 125 (MW/m^2) and λ_q^{fl} = 1/442.8 (m) = 2.26 (mm)

$q_{\|e}^{kcSp}(0)$ = 76 (MW/m^2) and λ_q^{kcSp} = 1/556.6 (m) = 1.80 (mm) .

4. Measured and Modelled Power Deposition Profiles on the Outer Target

For each shot, infrared thermographic measurements were made of the profile of the deposited power flux density on the outer target, $q_{\text{dep-ir}}$. From the values of the *deposited* power flux density the equivalent *parallel* power flux density $q_{\parallel\text{-ir}}$ was then calculated; this calculation takes into account (i) the angle between the target surface and the magnetic field at the target, and (ii) the total flux expansion between the target and the omp.

The two most prominent features of the $q_{\parallel\text{-ir}}$ profile are the magnitude of the peak, $q_{\parallel\text{-ir-peak}}$ and the location of this peak, specified as $\Delta R_{\text{ir-peak}} \equiv R^{\text{omp-std}}_{\text{ir-peak}} - R^{\text{omp-std}}_{\text{sep}}$, Table 4.

Table 4
Magnitude and location of the peak power deposition on the target, mapped to the omp.

Shot	$R^{\text{standard}}_{\text{sep}}$ (m)	$q_{\parallel - ir - peak}$ (MW/m^2)	$\Delta R_{\text{ir-peak}}$ (mm)	$P^{\text{rad}}_{\text{SOL}}$ (MW)	P^{SOL} (MW)	L_{conn} (m)	$(B_\theta / B)_{\text{omp}}$
144977	2.26677	24.7	1.30	0.68	2.16	20.8	0.193
144981	2.27048	31.0	0.87	0.80	2.34	14.4	0.110
144982	2.26920	30.6	0.88	0.80	2.34	14.4	0.182
144986	2.25675	11.7	1.90	0.48	2.04	39.8	0.180
144987	2.26283	11.4	2.01	0.46	2.06	39.5	0.186
144990	2.25596	41.8	0.78	1.03	3.06	20.4	0.264
144992	2.25626	43.3	0.76	0.98	2.79	20.5	0.262
144993	2.26469	43.2	0.72	1.14	3.30	20.4	0.108
144994	2.26223	22.6	0.57	0.97	2.16	14.3	0.248
145001	2.25542	17.8	1.48	0.71	2.31	29.2	0.133
145002	2.25551	18.4	1.47	0.72	2.42	29.2	0.134
148980	2.27067	24.6	0.91	0.95	3.57	19.9	0.196
148981	2.27038	20.2	0.86	0.84	3.28	19.7	0.199
148982	2.26778	33.4	1.09	1.70	5.64	19.6	0.204
148983	2.26957	59.6	1.05	1.43	6.16	19.4	0.214
148984	2.27000	52.6	1.08	1.42	6.47	19.5	0.212
148985	2.26972	74.9	1.31	2.13	7.78	19.6	0.200
148986	2.27273	72.5	1.54	2.16	8.73	19.3	0.213
148988	2.26994	26.1	0.80	0.93	3.8	18.8	0.201
148989	2.26655	18.0	1.06	0.89	3.95	19.8	0.204
148990	2.26595	17.6	1.03	0.87	3.78	19.2	0.203

Instead of using the ir-measured quantities, one can use target Langmuir probe data; however, this requires knowing the ratio of ion to electron temperature at the target; it also requires a reliable estimate for the sheath heat transmission coefficient, which has many contributing effects (Sec. 25.5 of Ref. 7).

While $q_{\parallel\text{-ir-peak}}$ and $\Delta R_{\text{ir-peak}}$ are the principal features of the target power profile, the entire profile can be fitted using the Eich procedure [9]. We now briefly recapitulate the Eich procedure since, as will be seen, it is particularly well suited to the present analysis.

"*By expressing the target coordinate as s and the strike line position on target as* s_0 *we describe the heat load profile at the divertor entrance as*

$$q_{\parallel}^{\text{Eich}}(\bar{s}) = q_{\parallel 0}^{\text{Eich}} \exp\left(-\frac{\bar{s}}{\lambda_q f_x}\right) \quad \text{and} \quad \bar{s} = s - s_0, \qquad s \geq s_0 \tag{8}$$

(superscript "Eich" added here)

This simple ansatz allows to account for perpendicular heat diffusion or leakage into the private-flux-region (PFR) by introducing a Gaussian width S representing the competition between parallel and perpendicular heat transport in the divertor volume. This means that, physically, the exponential profile at the divertor entrance, is diffused into the private flux region while travelling towards the target. This competition is approximated by a convolution of the exponential profile with a Gaussian function with the width S. The target heat flux profiles are thus expressed as

$$q_{\parallel}^{\text{Eich}}(\bar{s}) = \frac{q_{\parallel 0}^{\text{Eich}}}{\sqrt{\pi} S} \int_0^{\infty} \exp\left(-\bar{s}' / \lambda_q f_x\right) \exp\left(-(\bar{s} - \bar{s}') / S^2\right) d\bar{s}' + q_{\text{back-gnd}}$$

$$= \frac{q_{\parallel 0}^{\text{Eich}}}{2} \exp\left(\left(\frac{S}{2\lambda_q f_x}\right)^2 - \frac{\bar{s}}{\lambda_q f_x}\right) erfc\left(\frac{S}{2\lambda_q f_x} - \frac{\bar{s}}{S}\right) + q_{\text{back-gnd}} \quad ,$$

$$s, \bar{s} \in (-\infty, \infty) \tag{9}$$

(where f_x *is the total magnetic flux expansion between the target and the omp)*."

The exercise of fitting the ir power profiles to the Eich expression yields values of the fitting parameters $q_{\|0}^{\text{Eich}}$, λ_q^{Eich}, S, s_0 and $q_{b\text{-}g}$ for each shot. For the present work, the value of $q_{\|0}^{\text{Eich}}$ is of direct interest since we want to know whether it matches the theoretical electron parallel power flux density at the omp separatrix, $q_{\|e}^{\text{kcSp}}(R_{\text{sep}}^{\text{std}})$, (calculated using the Thomson $T_e(R_{\text{sep}}^{\text{std}})$ and $n_e(R_{\text{sep}}^{\text{std}})$), and if not, then we want to know how much shift of R_{sep} is required to achieve agreement.

We use here the more compact version of the Eich formulation given by Makowski [10]:

$$q_{\|}^{\text{Eich}}(\sigma) = \frac{q_{\|0}^{\text{Eich}}}{2} e^{\mu^2 - 2\mu\sigma} erfc(\mu - \sigma) \tag{10}$$

where $\sigma = \bar{s}/w$, w = S, $\mu = w/2\lambda$, $\lambda = \lambda_q f_x$ and $q_{b\text{-}g}$ has been neglected. For each shot in the data set the values of fitting parameters $q_{\|0}^{\text{Eich}}$, w, $\lambda\left(\equiv \lambda_q^{\text{Eich}}\right)$ and μ are given in Table 5. Some further aspects of the Eich procedure are considered in the Appendix.

The values of λ_q^X for all the shots are given in Table 6, and comparison is made with the ir-measured values, λ_q^{Eich}, in Fig. 4 where they are plotted vs I_p. As can be seen from Fig. 4, there is excellent agreement between λ_q^{Eich} and either $\lambda_q^{\text{flux-lim}}$ or $\lambda_q^{\text{kin-corr-Sp}}$.

As was reported earlier [10], λ_q^{fl} is closer, on average, to λ_q^{Eich} that is λ_q^{Sp}; however, λ_q^{kcSp} is closer still with $<\lambda_q^{\text{kcSp}}/\lambda_q^{\text{Eich}}>$ = 0.92. If shots 144986, 7 (whose cubic fits to the Thomson data have very poor statistics, Table 1) and shots 145001, 2 (which used ECRH heating) are omitted from the average, then $<\lambda_q^{\text{kcSp}}/\lambda_q^{\text{Eich}}>$ increases to 0.95.

Table 5
Eich fit parameters for the ir-measured power deposition profiles at the outer target.

Shot	$q_{\parallel 0}^{Eich}$ (MW/m^2)	w (mm)	λ_q^{Eich} (mm)	μ
144977	58.34	1.96	2.37	0.41
144981	60.12	1.10	1.91	0.29
144982	58.17	1.09	1.99	0.28
144986	34.60	3.50	3.00	0.58
144987	35.85	3.95	3.04	0.65
144990	77.26	0.94	1.95	0.24
144992	81.86	0.94	1.74	0.27
144993	76.74	0.84	1.78	0.23
144994	38.02	0.65	1.59	0.20
145001	29.45	1.61	4.05	0.20
145002	30.35	1.60	4.05	0.20
148980	65.16	1.50	1.51	0.50
148981	56.01	1.49	1.39	0.54
148982	81.70	1.68	1.91	0.44
148983	148.12	1.64	1.82	0.45
148984	127.41	1.66	1.92	0.43
148985	157.12	1.76	2.66	0.33
148986	145.29	1.99	3.31	0.30
148988	73.47	1.40	1.28	0.55
148989	43.40	1.63	1.89	0.43
148990	38.97	1.47	1.98	0.37

Table 6
Experimental (Eich) and model values for the exponential decay length of power width at the outer target, mapped to the omp.

Shot	λ_q^{Eich} (mm)	$\lambda_q^{flux\text{-}lim}$ (mm)	$\lambda_q^{Spitzer}$ (mm)	$\lambda_q^{kin\text{-}corr\text{-}Sp}$ (mm)	$\lambda_q^{flux\text{-}lim} / \lambda_q^{Eich}$	$\lambda_q^{Spitzer} / \lambda_q^{Eich}$	$\lambda_q^{kin\text{-}corr\text{-}Sp} / \lambda_q^{Eich}$
144977	2.37	2.26	1.44	1.80	0.95	0.60	0.76
144981	1.91	1.87	1.27	1.44	0.98	0.67	0.75
144982	1.99	1.72	1.10	1.27	0.87	0.55	0.64
144986	3.00	4.12	2.35	3.06	1.37	0.78	1.02
144987	3.04	4.60	2.51	3.60	1.51	0.82	1.18
144990	1.95	2.66	1.47	1.99	1.37	0.76	1.02
144992	1.74	3.27	1.79	2.36	1.88	1.03	1.36
144993	1.78	2.32	1.35	1.74	1.30	0.76	0.98
144994	1.59	2.20	1.46	1.68	1.39	0.92	1.06
145001	4.05	2.38	1.32	1.72	0.59	0.33	0.42
145002	4.05	2.86	1.62	2.14	0.71	0.40	0.53
148980	1.51	2.14	1.25	1.70	1.41	0.83	1.13
148981	1.39	1.91	1.10	1.56	1.37	0.79	1.12
148982	1.91	2.25	1.29	1.84	1.18	0.67	0.96
148983	1.82	2.45	1.37	1.97	1.35	0.75	1.08
148984	1.92	2.31	1.26	1.89	1.20	0.65	0.98
148985	2.66	2.49	1.43	2.06	0.93	0.54	0.77
148986	3.31	2.58	1.32	2.16	0.78	0.40	0.65
148988	1.28	2.10	1.15	1.69	1.64	0.90	1.33
148989	1.89	1.96	1.19	1.62	1.03	0.63	0.86
148990	1.98	1.81	1.03	1.44	0.92	0.52	0.73
Average					1.18	0.68	0.92
Std. dev.					0.33	0.18	0.25

As theoretically expected, the kinetic-corrected-Spitzer parallel electron power flux density model is closest to measurements of deposited power width on the outer target, therefore in the remainder of the paper this power flux assumption will be used to identify the location of the omp separatrix based on power accounting.

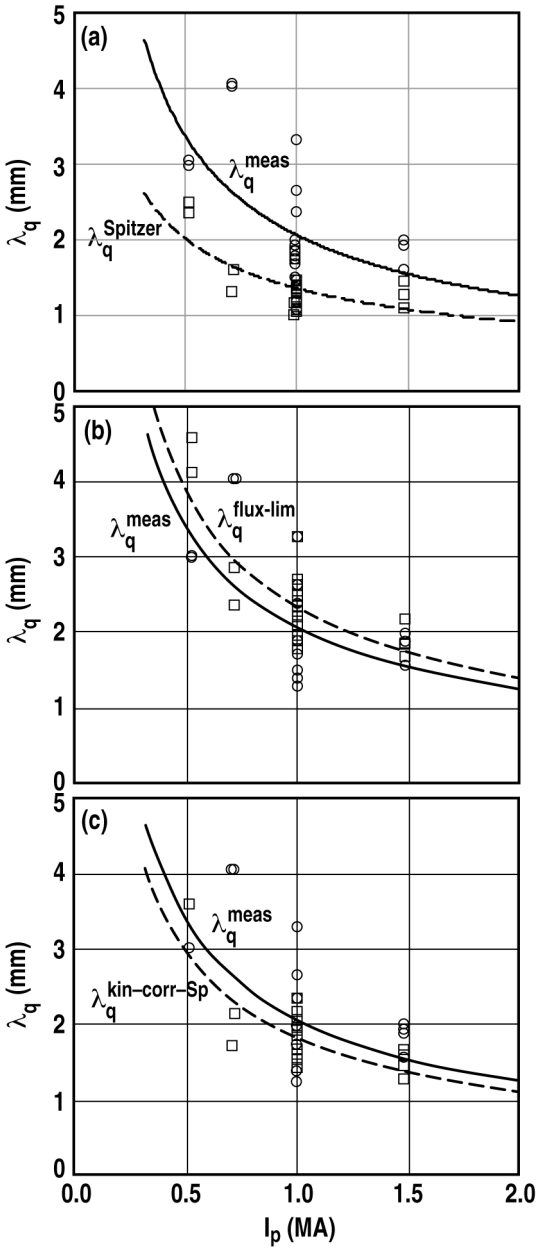

Fig. 4. Comparison of ir-measured (Eich) λ_q^{meas} (circles) and model (squares) exponential power widths at the target, mapped to omp, plotted as a function of plasma current, I_p. The solid (measured) and dashed (model) lines are the best-fit power functions for I_p (MA), λ [mm]: $\lambda_q^{meas}=2.07I_p^{-0.71}$ ($R^2 = 0.36$); $\lambda_q^{Spitzer}=1.36I_p^{-0.57}$ ($R^2 = 0.48$); $\lambda_q^{flux-lim}=2.34I_p^{-0.72}$ ($R^2 = 0.63$); $\lambda_q^{kin-corr-Sp}=1.83I_p^{-0.70}$ ($R^2 = 0.63$).

5. The $P_{SOL}^{exhaust}$ Method Based On $q_{deposited}^{target}$, the Measured Target Power Flux Density

5.1 The $P_{SOL}^{exhaust}$ Method applied to the DIII-D discharges

The basic idea of the $P_{SOL}^{exhaust}$ Method is to compare the ir-measured power profile at the outer target (after it is converted to a parallel power flux density and mapped back to the omp) with the theoretical one based on kinetically-corrected Spitzer electron heat conduction calculated at the omp from the measured Thomson profiles. Conceptually, the most straightforward comparison is of $q_{||0}^{Eich}$ with $q_{||e}^{kcSp}(R_{sep}^{std})$, i.e. the power flux densities at the *separatrix*; we will call this $P_{SOL}^{exhaust}$ Method A. Alternatively the comparison can be made of $q_{||\text{-ir-peak}}$ with $q_{||e}^{kcSp}(R_{ir\text{-}peak}^{std})$, i.e. at the *peak*; we will call this $P_{SOL}^{exhaust}$ Method B. Method B has the disadvantage that the quality of the Thomson data is poorer at $R_{ir\text{-}peak}^{std}$ than at R_{sep}^{std}: generally with increasing R the number of data points decreases and the scatter increases. Apparently due to that, it was found that Method B failed to find a solution for about 30% of the cases, while Method A always produced a solution. For the cases where Method B provided a solution the required shift was found to differ little from Method A. $P_{SOL}^{exhaust}$ Method A was therefore used in the following to analyze the DIII-D discharges.

Here we only need to use the *shape* of the Eich profile, i.e. only the values of the Eich fitting parameters in Table 5, $q_{||0}^{Eich}$, w, λ and μ. This is sufficient to identify the location of the separatrix at the omp. One could also use the value of the Eich fitting parameter s_0, which would then identify the location of the separatrix at the outer strike point, providing a correction to the EFIT-identified location.

In order to take into account the volumetric power loss that occurs in the outer SOL between the omp, where $q_{\|e}^{kcSp}$ applies, and the target, where $q_{\|0\text{-ir}}\left(\equiv q_{\|0}^{Eich}\right)$ applies, we will define a *power-loss-corrected separatrix target power flux density*:

$$q_{\|0\text{-ir}}^{pwr\text{-}ls\text{-}corr} \equiv q_{\|0\text{-ir}} / \left(1 - P_{SOL}^{rad} / P_{SOL}\right) \tag{11}$$

where P_{SOL}^{rad} and P_{SOL} were measured for each shot using bolometry, Table 4. P_{SOL} is the difference between the heating power and the power radiated inside the separatrix, measured by bolometry. P_{SOL}^{rad} is the bolometric power loss from the lower divertor which is assumed here to be the total volumetric power loss from the SOL for these lower single-null discharges.

For $P_{SOL}^{exhaust}$ Method A we then compare $q_{\|e}^{kcSp}(R - R_{sep}^{std})$ with $q_{\|0\text{-ir}}^{pwr\text{-}ls\text{-}corr}$. This is shown in Fig. 3 for the example of shot 144977 for which $q_{\|0\text{-ir}}^{pwr\text{-}ls\text{-}corr}$ = 85 MW/m^2. The shifts of the separatrix relative to R_{sep}^{std} required for power accounting are: for Spitzer: +1.17 mm; for flux-limited: +0.82 mm; for kinetic-corrected Spitzer: -0.18 mm. (The shift moves the vertical axis at 0 in Fig. 3 so that it passes through the intersection of the curved line and the horizontal dashed line.)

Table 7 gives the required shifts of the separatrix relative to R_{sep}^{std} for all the shots for $P_{SOL}^{exhaust}$ Method A, for kinetically-corrected-Spitzer parallel electron heat conduction.

It should be noted, that in comparing $q_{\|e}^{X}(R - R_{sep}^{std})$ with $q_{\|\text{-ir}}^{pwr\text{-}ls\text{-}corr}$ we are assuming that the latter is due purely to the *electron* power transport along the SOL, and that the *ion* contribution can be neglected. This is expected to be approximately true when:

(a) the electrons and ions are thermally decoupled in the SOL

(b) the ion power width is significantly greater than the electron power width.

Table 7

The $P_{SOL}^{exhaust}$ Method A applied to the set of DIII-D discharges for kinetically-corrected-Spitzer electron heat conduction. Shifts of the separatrix relative to R_{sep}^{std} required for power accounting, in [mm]. It may be noted that the average shift is only -0.12 mm, which is small compared with the average standard shift $\langle \Delta R_{sep}^{std} \rangle$ = -2.02 mm, see Table 1. The average total shift is -2.14 mm relative to the EFIT value.

Discharge	Req'd shift of separatrix (mm)	Discharge	Req'd shift of separatrix (mm)
144977	-0.18	148980	0.13
144981	-1.17	148981	1.00
144982	-0.98	148982	0.21
144986	-0.84	148983	-0.62
144987	0.50	148984	-0.21
144990	-1.20	148985	-0.14
144992	-1.77	148986	1.07
144993	-0.47	148988	0.72
144994	-1.41	148989	0.84
145001	0.20	148990	1.12
145002	0.63		
		Average	-0.12
		Std. dev.	0.88

This matter is discussed in Sec 4.4 of [7], where it is argued that (b) is likely to be true, although the database for λ_T is sparse. Table 3 of [2] also shows that for SOL's with collisionality $\nu_{omp}^{*e} \sim$ 5-15, which is the range for the present discharges, i.e. when the SOL is in the *conduction limited regime*, then T_e and T_i generally differ appreciably even at the target. When (b) is true then the contribution of the ions to $q_{\|\text{-ir}}^{\text{pwr-ls-corr}}$ is not great, unless the ion power entering the SOL, P_{SOL}^{i}, greatly exceeds the electron power entering the SOL, P_{SOL}^{e}; unfortunately not very much is known about this aspect of tokamak behaviour. In Sec. 5(b) we apply the $P_{SOL}^{exhaust}$ Method to *calculated* SOLPS solutions for a number of FDF tokamak cases in the conduction limited regime. For such

solutions the location of the omp separatrix is known exactly, of course, and thus light can be shed on the assumption that $q_{\|\text{-ir}}^{\text{pwr-ls-corr}}$ is due to the electron power transport along the SOL to a good approximation. It will be shown in Sec. 5.2 that this, in fact, is a good approximation – at least based on this comparison with code-calculated plasma solutions.

It is also expected that in the main SOL, e.g. near the omp, electron parallel heat *convection* will be small compared with electron parallel heat *conduction* – because of the very high electron heat conduction coefficient when T_e exceeds a few ten's eV, which is typical of the omp near the separatrix.

5.2 The $P_{SOL}^{exhaust}$ Method applied to SOLPS code-calculated cases

The $P_{\text{SOL}}^{\text{exhaust}}$ Method B was applied to the output from SOLPS code runs reported in [2] for the FDF tokamak. Since there is no issue involved here about poor quality Thomson data at large R, and no risk of failed solutions, then $P_{\text{SOL}}^{\text{exhaust}}$ Method B is preferred over A, since the primary input – the target power profile – is used directly. For Case 11 of [2], the deposited power flux density on the outer target is shown in Fig. 5.

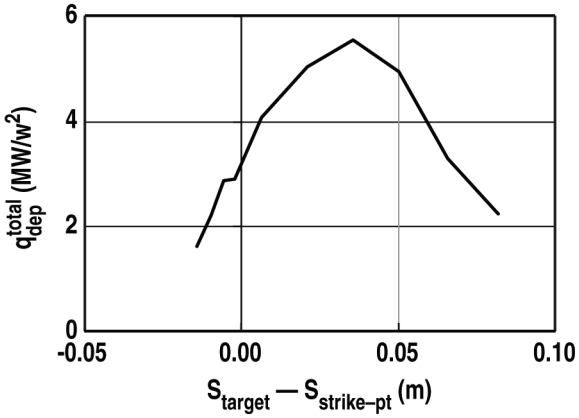

Fig. 5. For SOLPS-calculated FDF Case 11 [2]. The total deposited power flux density at the outer target, including both the plasma heat deposition and the radiative power deposition. The horizontal axis gives the location across the target. In order to map the profile to the omp, the effect of flux expansion has to be included which will reduce the power flux density at the omp by the total magnetic flux expansion factor $R_{\text{target-strike-pt}}/R_{\text{omp-sep}} = 2.292\text{m}/3.19\text{m} = 0.718$. Also the pitch angle of the field at the target, ~ 1 degree, has to be used to obtain the implied parallel power flux density.

Using Fig. 5, we can obtain the location of the power peak on the target and its magnitude, $R_{\text{peak}}^{\text{omp}} - R_{\text{sep}}^{\text{omp}}$ and $q_{\|\text{-peak}}$, as needed for the application of the $P_{\text{SOL}}^{\text{exhaust}}$ Method B. We also need to allow for

volumetric power loss in the outer SOL: $q_{\|\text{-peak}}^{\text{pwr-ls-corr}} \equiv q_{\|\text{-peak}} / \left(1 - P_{\text{vol-loss}} / P_{\text{SOL}}^{\text{input}}\right)$. For Case 11 the SOLPS-calculated values are: $P_{\text{SOL}}^{\text{input}}$ = 31.7 MW, $P_{\text{rad-SOL}}$ = 16.4 MW, $P_{\text{CX-SOL}}$ = -2.2. (i.e. there is volumetric CX heating rather than cooling), $P_{\text{target}}^{\text{rad}}$ = 5.7 MW (total radiative power loss to target), thus $P_{\text{vol-loss}} / P_{\text{SOL}}^{\text{input}}$ = (16.4 - 2.2 - 5.7)/31.7 = 0.269. Note that $P_{\text{target}}^{\text{rad}}$ has to be subtracted here in order to avoid double-counting, since the value of $q_{\|\text{-peak}}$ used here includes the radiative load. Experimentally the latter is always included in the measured target load. For code-calculated solutions one can separate out the part of $q_{\|\text{-peak}}$ that is due to the plasma contact alone and use that, in which case $P_{\text{target}}^{\text{rad}}$ should not be included in $P_{\text{vol-loss}} / P_{\text{SOL}}^{\text{input}}$. When that is done here, it gives virtually the same result for $q_{\|\text{-peak-total}}^{\text{pwr-ls-corr}}$, namely 284 MW/m^2.

Note that the subscript "total" has been added to indicate that the total plasma heat deposition due to both electrons and ions has been included here (as well as the radiative load). Although the information is not available for experimental situations, for code-calculated cases we have the information needed to calculate $q_{\|\text{-peak-e}}^{\text{pwr-ls-corr}}$, where the subscript "e" indicates that only the plasma heat deposition due to electrons has been included (plus the radiative load), here giving $q_{\|\text{-peak-e}}^{\text{pwr-ls-corr}}$ = 178 MW/m^2.

For Case 11 the peak location is $R_{\text{peak}}^{\text{omp}} - R_{\text{sep}}^{\text{omp}}$ = 1.15 mm. We thus have all the information needed to apply the $P_{\text{SOL}}^{\text{exhaust}}$ Method B; results are shown in Fig. 6. As noted earlier, the SOLPS code uses kinetically-corrected-Spitzer parallel electron heat transport.

The shifts required to be applied to the code-simulated Thomson profiles for other Cases from [2] are summarized in Table 8. From this it is concluded that, based on these SOLPS cases, it is a good assumption to assign all of the deposited power on the target to the electron parallel power flux upstream, at least at locations near the peak deposited power.

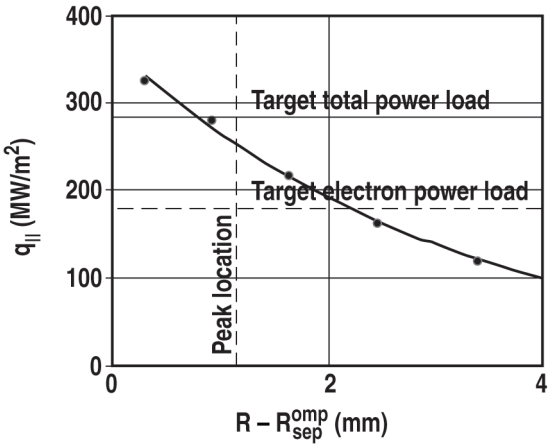

Fig. 6. The $P_{SOL}^{exhaust}$ Method B applied to SOLPS FDF Case 11 in Ref. [2]. If it is assumed that the electron parallel power flux has to carry *all* of the target power load (284 MW/m^2, solid horizontal line) at the peak location (the vertical dashed line), then the code-simulated Thomson profile (curve with dots) would have to be shifted outward by 0.35 mm, while if it assumed that it has to carry *only the electron part* of the peak target load (178 MW/m^2, dashed horizontal line), then the required shift would be inward by 0.84 mm.

Table 8

Required shifts from application of the $P_{SOL}^{exhaust}$ Method B to SOLPS FDF solutions [2]. As can be seen, the assumption that the parallel electron power flux density provides $q_{\parallel\text{-peak-total}}^{\text{pwr-ls-corr}}$ for these conduction-limited code-calculated cases is quite good. The required shift, on average, is 0.10 mm which is effectively zero since it is smaller than the standard deviation of the shifts 0.26 mm.

SOLPS FDF Case, Ref. [2]	Required Shift (mm) Assuming $q_{\parallel\text{-peak-total}}^{\text{pwr-ls-corr}}$	Required Shift (mm) Assuming $q_{\parallel\text{-peak-electron}}^{\text{pwr-ls-corr}}$
8	-0.19	-0.84
9	0.09	-0.84
10	-0.33	-1.44
11	0.35	-0.84
12	0.37	-0.40
13	0.47	-0.79
14	0.07	-0.93
17	0.07	-0.40
26	0.00	-0.93
Average	0.10	-0.82
Standard deviation	0.26	0.31

6. The P_{SOL}^{input} Method, a Method Based on the Measured Power into the SOL

6.1 The P_{SOL}^{input} Method applied to the DIII-D discharges

For the P_{SOL}^{input} Method, instead of the primary experimental input being the measured power profile at the outer target, $q_{deposited}^{target}$, it is now the power entering the SOL, P_{SOL}. Here we identify the location of the omp-separatrix by comparing $q_{||e}^{kcSp}(R - R_{sep}^{std})$ with $q_{||\text{-sep-power-bal}}^{kcSp}$ where:

$$q_{||\text{e-sep-power-bal}}^{kcSp} \equiv \frac{P_{SOL}^{e}}{4\pi R_{\text{sep-omp}} \lambda_{q_e}^{kcSp} (B_\theta / B)_{omp}} \quad . \tag{12}$$

We use the same convenient exponential-fit approximation as for the $P_{SOL}^{exhaust}$ Method, $q_{||e}^{kcSp}(R - R_{sep}^{std}) = q_{||0}^{kcSp}(0)\exp[-(R - R_{sep}^{std}) / \lambda_q^{kcSp}]$.

We need to know the value for P_{SOL}^{e}, the power entering the outer SOL carried by electrons. This quantity is not available experimentally; only P_{SOL} is available, the total carried by electrons and ions. We will define $fp_e \equiv P_{SOL}^{e} / (P_{SOL}^{e} + P_{SOL}^{i}) \equiv P_{SOL}^{e} / P_{SOL}$ as the fraction of the total power carried by electrons in the main part of the SOL. In Sec. 6.2 the P_{SOL}^{input} Method is applied to the same SOLPS FDF cases as in Sec. 5.2 giving an average value for the 11 cases of $fp_e = 0.569$. We will round this to $fp_e = 0.5$ to apply to the DIII-D discharges.

Table 1 gives the values of the parameters needed to evaluate equation (12). For shot 144977 this gives $q_{||\text{-sep-power-bal}}^{kcSp} = 109$ MW/m^2. We then obtain the required shifts of the Thomson data, ΔR^{kcSp}, by setting:

$$q_{||0}^{kcSp}(0)\exp\left[\Delta R^{kcSp} / \lambda_q^{kcSp}\right] = q_{||\text{-sep-power-bal}}^{kcSp} \quad . \tag{13}$$

This gives $\Delta R^{\mathrm{kcSp}} = 0.64$ mm, i.e. the Thomson data should be moved outward by 0.64 mm or equivalently the separatrix should be moved inward by 0.64 mm, i.e. $R_{\mathrm{sep}}^{\mathrm{correct}} = R_{\mathrm{sep}}^{\mathrm{standard}} - 0.64$ mm. Results for all of the shots are given in Table 9.

Table 9

The $P_{\mathrm{SOL}}^{\mathrm{input}}$ Method applied to the set of DIII-D discharges. Shifts of the separatrix relative to $R_{\mathrm{sep}}^{\mathrm{std}}$ required for power accounting, in [mm]. It may be noted that the average shift is -1.40 mm, which is smaller than the average standard shift $\left\langle \Delta R_{\mathrm{sep}}^{\mathrm{std}} \right\rangle$ = -2.02 mm, see Table 1. The average total shift is -3.42 mm relative to the EFIT value.

Shot	P_{SOL} (MW)	Req'd Shift of Separatrix (mm)	Shot	P_{SOL} (MW)	Req'd Shift of Separatrix
144977	2.16	-0.64	148980	3.57	-1.15
144981	2.34	-1.42	148981	3.28	-0.43
144982	2.34	-1.42	148982	5.64	-1.26
144986	2.04	-3.55	148983	6.16	-1.16
144987	2.06	-2.05	148984	6.47	-1.21
144990	3.06	-1.87	148985	7.78	-1.08
144992	2.79	-1.97	148986	8.73	-0.12
144993	3.3	-1.20	148988	3.8	-0.51
144994	2.16	-1.89	148989	3.95	-1.28
145001	2.31	-2.23	148990	3.78	-1.04
145002	2.42	-1.99			
			Average		-1.40
			Std. dev		0.75

6.2 The $P_{\mathrm{SOL}}^{\mathrm{input}}$ Method applied to SOLPS code-calculated cases

The values of n_e(R) and T_e(R) are taken from the SOLPS output [2] at the omp, also the values of $R\left(B_\theta / B_\varphi\right)$ for each grid point. Here in place of $P_{\mathrm{SOL}}^{\mathrm{expt}}$ we will use the code value of $P_{\mathrm{SOL}}^{\mathrm{SOLPS}}$ or some specified fraction, fp_e, of $P_{\mathrm{SOL}}^{\mathrm{SOLPS}}$; the former assumes that all of the e + i power entering the SOL is carried away by electron parallel heat conduction,

while the 2nd assumes that only the fraction fp_e is so carried; we want to find the value of fp_e required to give the exact known location of the omp separatrix when applying the P_{SOL}^{input} Method.

Since SOLPS uses $q_{||}^{kcSpitzer}(R)$, that is used here.

For the FDF magnetic configuration $(B_\theta / B)_{omp} = 0.356$ and $R_{sep\text{-}omp} = 3.19$ m. For the Case 11 of [2] $P_{SOL}^{SOLPS} = 31.7$ MW also $q_{||0}^{kcSp} = 364.6$ MWm^2 and $\lambda_q^{kcSp} = 3.07$ mm. Thus

$$q_{||e\text{-}sep\text{-}power\text{-}bal}^{kcSp} = \frac{f_{P_e} P_{SOL}}{4\pi R_{sep\text{-}omp} \lambda_q^{kcSp} (B_\theta / B)_{omp}} = 723.6\, fp_e$$

which we set equal to 364.6 thus obtaining $fp_e = 0.504$. Results for the other cases are shown in Table 10. As noted earlier, the average value for the 11 cases is 0.569.

Table 10

Results of application of the $P_{\mathrm{SOL}}^{\mathrm{input}}$ Method to SOLPS-calculated cases where the exact location of the omp separatrix is known. $\left\langle \nu_{\mathrm{omp}}^{*\mathrm{e}} \right\rangle$ is the value of the electron collisionality, evaluated at the omp and averaged over the first 3.3. mm into the SOL. For comparison, the values for $\left\langle \nu_{\mathrm{omp}}^{*\mathrm{e}} \right\rangle$ for the set of DIII-D discharges spanned 2 – 12, i.e. essentially the same range.

SOLPS FDF Case	$\chi_{\perp e}, \chi_{\perp i}$ (m^2/s)	$P_{\mathrm{SOL}}^{\mathrm{e}} / P_{\mathrm{SOL}}$	$\left\langle \nu_{omp}^{*e} \right\rangle$	f_{P_e}
5	1, 1		4.80	0.666
6	1, 1		11.3	0.524
8	1, 1	0.56	5.3	0.707
9	1, 1	0.55	13.2	0.516
10	2, 2	0.58	4.90	0.662
11	2, 2	0.56	13.0	0.504
12	1, 3	0.47	12.5	0.469
13	3, 1	0.71	11.9	0.616
14	3, 0.3	0.84	12.5	0.697
17	0.3, 3	0.39	13.0	0.414
26	0.3, 0.3	0.50	15.6	0.484
Average				0.569
Std. dev.				0.103

7. Comparison of the R_{sep} Values Obtained from the Two Power Accounting Methods

In Table 11 the required shifts of R_{sep} are compared for the $P_{SOL}^{exhaust}$ Method A and the P_{SOL}^{input} Method. In Tables 12 and 13, the values of n_e and T_e at the corrected separatrix location for kinetically-corrected-Spitzer are given for each shot, for the 2 Methods.

Table 11

The difference in the required shifts of R_{sep} relative to R_{sep}^{std} for the two Methods.

Shot	Difference in Req'd Shifts: $P_{SOL\text{-}exhaust}$ Meth. - $P_{SOL\text{-}input}$ Meth (mm)	Shot	Difference in Req'd shifts: $P_{SOL\text{-}exhaust}$ Meth. - $P_{SOL\text{-}input}$ Meth (mm)
144977	0.46	148980	1.28
144981	0.25	148981	1.43
144982	0.44	148982	1.47
144986	2.71	148983	0.54
144987	2.55	148984	1.00
144990	0.67	148985	0.94
144992	0.20	148986	1.19
144993	0.73	148988	1.23
144994	0.48	148989	2.12
145001	2.43	148990	2.16
145002	2.62		
		Average	1.28
		Std. dev	0.84

Table 12

The values of n_e^{sep} after the required shifts of R_{sep} relative to R_{sep}^{std} have been applied to satisfy power accounting, for the two Methods, and comparison with the values from the standard method.

Shot	Standard Method	$P_{SOL}^{exhaust}$ Method	P_{SOL}^{input} Method	Avg of $P_{SOL}^{exhaust}$ & P_{SOL}^{input}	Normalized Difference $P_{SOL}^{exhaust}$ - P_{SOL}^{input}	Difference Std - $\langle n_e^{sep} \rangle$ (10^{18} m^{-3})	Normalized Difference Std - $\langle n_e^{sep} \rangle$
	n_e^{sep} (10^{18} m^{-3})	n_e^{sep} (10^{18} m^{-3})	n_e^{sep} (10^{18} m^{-3})	$\langle n_e^{sep} \rangle$ (10^{18} m^{-3})	$\lvert \Delta n_e^{sep} \rvert \langle n_e^{sep} \rangle$		$\lvert \Delta n_e^{sep} \rvert$/std
144977	8.4	8.6	9.3	9.0	0.08	-0.5	-0.07
144981	15.2	19	20	19.5	0.05	-4.3	-0.28
144982	15.4	18.5	20.1	19.3	0.08	-3.9	-0.25
144986	4.9	5.1	6.3	5.7	0.21	-0.8	-0.16
144987	4.3	4.2	4.7	4.5	0.11	-0.2	-0.03
144990	6.6	7.4	7.9	7.7	0.07	-1.1	-0.16
144992	7.1	8.6	8.8	8.7	0.02	-1.6	-0.23
144993	9.1	9.7	10.6	10.2	0.09	-1.1	-0.12
144994	11.5	14.4	15.4	14.9	0.07	-3.4	-0.30
145001	7.2	7.1	9	8.1	0.24	-0.9	-0.12
145002	5.9	6.8	8.5	7.7	0.22	-1.8	-0.30
148980	9.0	8.8	10.3	9.6	0.16	-0.6	-0.06
148981	9.5	8.4	10	9.2	0.17	0.3	0.03
148982	9.2	9	10.6	9.8	0.16	-0.6	-0.07
148983	10.0	10.6	11.1	10.9	0.05	-0.9	-0.09
148984	8.9	9.1	10	9.6	0.09	-0.7	-0.07
148985	11.0	11.2	12.3	11.8	0.09	-0.8	-0.07
148986	10.8	10.2	10.9	10.6	0.07	0.3	0.02
148988	9.2	8.6	9.7	9.2	0.12	0.1	0.01
148989	8.0	7.1	9.8	8.5	0.32	-0.4	-0.06
148990	9.1	8	10.4	9.2	0.26	-0.1	-0.01
Avg.					0.13		-0.11
Std. Dev.					0.08		0.10

Table 13

The values of T_e^{sep} after the required shifts of R_{sep} relative to R_{sep}^{std} have been applied to satisfy power accounting, for the two Methods, and comparison with the values from the standard method.

Shot	Standard Method	$P_{SOL}^{exhaust}$ Method	P_{SOL}^{input} Method	Avg of $P_{SOL}^{exhaust}$ & P_{SOL}^{input}	normalized difference $P_{SOL}^{exhaust}$ - P_{SOL}^{input}	difference std - $\langle T_e^{sep} \rangle$	normalized difference std - $\langle T_e^{sep} \rangle$
	T_e^{sep}	T_e^{sep}	T_e^{sep}	$\langle T_e^{sep} \rangle$	$\lvert \Delta T_e^{sep} \rvert / \langle T_e^{sep} \rangle$		$\lvert \Delta T_e^{sep} \rvert$/std
	(eV)	(eV)	(eV)	(eV)		(eV)	
144977	82	85	94	90	0.10	-7.5	-0.09
144981	51	68	73	71	0.07	-19.5	-0.38
144982	51	68	77	73	0.12	-21.5	-0.42
144986	75	83	113	98	0.31	-23.0	-0.31
144987	94	89	116	103	0.26	-8.5	-0.09
144990	77	103	122	113	0.17	-35.5	-0.46
144992	70	102	107	105	0.05	-34.5	-0.49
144993	86	95	111	103	0.16	-17.0	-0.20
144994	48	64	71	68	0.10	-19.5	-0.41
145001	74	71	123	97	0.54	-23.0	-0.31
145002	51	72	117	95	0.48	-43.5	-0.85
148980	88	85	116	101	0.31	-12.5	-0.14
148981	108	81	120	101	0.39	7.5	0.07
148982	101	96	136	116	0.34	-15.0	-0.15
148983	101	116	131	124	0.12	-22.5	-0.22
148984	107	113	145	129	0.25	-22.0	-0.21
148985	117	120	145	133	0.19	-15.5	-0.13
148986	151	117	155	136	0.28	15.0	0.10
148988	108	89	123	106	0.32	2.0	0.02
148989	90	7	125	66	1.79	24.0	0.27
148990	94	68	126	97	0.60	-3.0	-0.03
Average					0.33		-0.21
Std. Dev.					0.37		0.25

8. Sensitivity Analysis

In this section, we examine the effect on the deduced value of R_{sep} of varying the main assumptions in the foregoing analysis.

8.1 The effect of varying Z_{eff}^{SOL} on $q_{\|e}^{Sp}$ and $q_{\|e}^{kcSp}$

The Spitzer heat conduction coefficient κ_{0e} depends on Z_{eff}^{SOL}, which is not measured in the SOL; however, as can be seen from Fig. 7, the required shift only changes by ~ 0.3 mm as Z_{eff}^{SOL} is varied from 1 to 2. The reason for this insensitivity is, as referred to earlier, that $q_{\|e}^{Sp}$ is a very rapidly decreasing functions of $(R - R_{sep}^{std})$. There is thus also only a weak dependence on the value assumed for Z_{eff}^{SOL} in the Spitzer power flux coefficient $\kappa_{0e}\left(Z_{eff}^{SOL}\right)$.

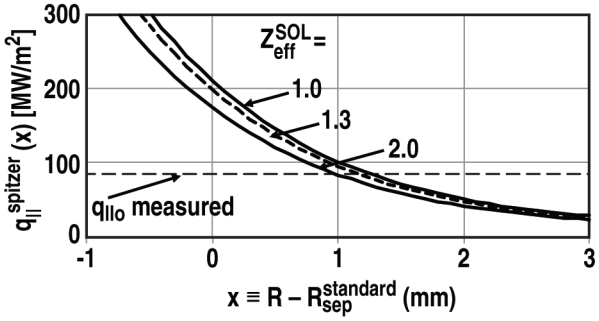

Fig. 7. The $P_{SOL}^{exhaust}$ Method A applied to DIII-D discharge 144977. There is only a weak dependence of the required shift of R_{sep} relative to R_{sep}^{std} on the value assumed for Z_{eff}^{SOL} in the Spitzer power flux coefficient $\kappa_{0e}\left(Z_{eff}^{SOL}\right)$. The required shift only changes by ~ 0.3 mm as Z_{eff}^{SOL} is varied from 1 to 2.

8.2 The effect on R_{sep} of varying α_e on $q_{\|e}^{fl}$ and $q_{\|e}^{kcSp}$

For flux-limited heat conduction, the value of the coefficient α_e is not accurately known; however, the required shift of the separatrix only changes by ~ $\pm$ 0.7 mm as α_e is varied by $\pm$ 1/3 (Fig. 8). As before, the reason for this insensitivity is that $q_{\|e}^{fl}$ is a very rapidly decreasing functions of $(R - R_{sep}^{std})$.

8.3 *The effect on R_{sep} of changing the model for $q_{\|e}$ in the $P_{SOL}^{exhaust}$ Method*

As noted in Sec. 3, at least mathematically, $q_{\|e}^{Sp}$ and $q_{\|e}^{fl}$ represent the two limits of $q_{\|e}^{kcSp}$. We next consider the effect on the value for R_{sep} deduced using the $P_{SOL}^{exhaust}$ Method of Sec. 5 when these limits are assumed instead of $q_{\|e}^{kcSp}$. For kinetically-corrected Spitzer the shift average (std. dev.) = - 0.12 (0.88) mm, Table 5; for Spitzer the shift average (std. dev.) = 1.26 (0.99) mm; for flux-limited the shift average (std. dev.) = 1.06 (0.99) mm. Thus the difference, on average, for the deduced value of R_{sep} is ~ 1 mm, which is approximately the size of the standard deviations for each of the $q_{\|e}$-models. Again, this insensitivity is due to the fact that all of the $q_{\|e}^{X}$ are rapidly decreasing functions of $(R - R_{sep}^{std})$.

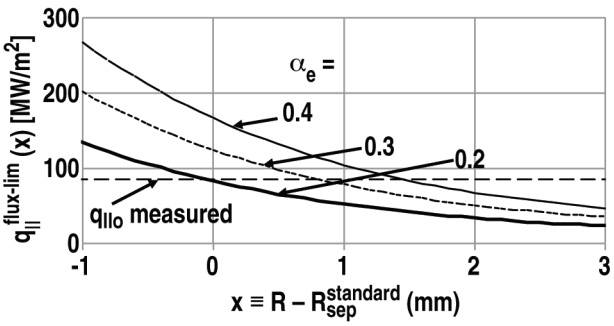

Fig. 8. The $P_{SOL}^{exhaust}$ Method A applied to DIII-D discharge 144977. There is only a weak dependence of the required shift of R_{sep} relative to R_{sep}^{std} on the value assumed for α_e : it only changes by $\sim \pm 0.7$ mm as α_e is varied by $\pm$ 1/3.

8.4 *The effect on R_{sep} of changing the model for $q_{\|e}$ in the P_{SOL}^{input} Method*

We next consider the effect on the value for R_{sep} deduced using the P_{SOL}^{input} Method of Sec. 6 when the $q_{\|e}^{Sp}$ and $q_{\|e}^{fl}$ limits are assumed instead of $q_{\|e}^{kcSp}$. For kinetically-corrected Spitzer the shift average (std. dev.) = - 1.40 (0.75) mm, Table 5; for Spitzer the shift average (std. dev.) = - 0.05 (0.74) mm; for flux-limited the shift average (std. dev.) = 0.07 (0.50) mm. Thus the difference, on average, for the deduced value of R_{sep} is again ~ 1 mm, which is approximately the size as the standard deviations for each of the $q_{\|e}$-models. Again, this insensitivity is due to the fact that all of the $q_{\|e}^{X}$ are rapidly decreasing functions of $(R - R_{sep}^{std})$.

8.5 The effect of changing the model for $q_{\|e}$ on the difference in the required shifts for the two Methods

It doesn't make a large difference if, instead of kinetically-corrected-Spitzer electron heat conduction, Spitzer or flux-limited is assumed: for kcSpitzer the shift average (std. dev.) = 1.28 (0.84) mm; for Spitzer the shift average (std. dev.) = 1.31 (0.74) mm; for flux-limited the shift average (std. dev.) = 0.99 (1.13) mm. The differences are small compared with the standard deviations.

8.6 The effect of varying P_{SOL} and f_{P_e} in the P_{SOL}^{input} Method

In order to apply the $P_{\mathrm{SOL}}^{\mathrm{input}}$ Method of Sec. 6, we need an input value for $P_{\mathrm{SOL}}^{\mathrm{e}} \equiv f_{P_e} P_{\mathrm{SOL}}$, equation (12). There is experimental error/uncertainty in the value of P_{SOL}. The value used for fp_{e}, 0.5, was found by applying the $P_{\mathrm{SOL}}^{\mathrm{input}}$ Method to SOLPS code-calculated cases, but there is some uncertainty involved in applying this to DIII-D experimental cases. Since it is the product $fp_{\mathrm{e}} P_{\mathrm{SOL}}$ that enters into equation (12) we next consider the effect of varying the value of this product. The extracted value of R_{sep} is not strongly dependent on the value $fp_{\mathrm{e}} P_{\mathrm{SOL}}$ that is used: increasing it by 30% changes the average shift of R_{sep} relative to $R_{\mathrm{sep}}^{\mathrm{std}}$ from -1.40 mm to -1.91 mm; decreasing it by 30% changes the average shift to - 0.71 mm. These differences are approximately the same as the standard deviation, 0.75 mm.

9. Discussion and Conclusions

The two power accounting methods give values for R_{sep} that differ rather little from each other, about 1 mm, Table 7. Since the two methods use quite different input, this increases confidence in this approach for identifying the omp separatrix location.

The two power accounting methods are rather robust regarding basic physics assumptions, specifically the model for the parallel electron conducted power. If instead of using the standard assumption of kinetically-corrected Spitzer heat conductivity, either of the extreme assumptions of pure Spitzer conduction (strong collisionality) or flux-limited conduction (weak collisionality) are used in the analysis, the extracted values of R_{sep} only change by about 1 mm, Tables 5 and 6.

The two power accounting methods give values of R_{sep} that differ little from the values obtained using the "standard DIII-D method" [6], also by about 1 mm, Tables 5 and 6. This results in only modest changes to the values of n_e and T_e at the omp separatrix relative to the "standard" values, increasing n_e^{sep} by ~ 10% and T_e^{sep} by ~ 20%, Tables 12 and 13.

10. References

[1] Makowski MA *et al* "Scaling of the Divertor Heat Flux Width in the DIII-D Tokamak and Its Relation to Upstream Profiles" to be submitted to *Nucl. Fusion*

[2] Stangeby PC, Canik JM and Whyte DG, 2010 *Nucl. Fusion* **50** 125003

[3] Chan VS *et al* 2011 *Nucl. Fusion* **51** 083019

[4] Carlstrom TN *et al* 1992 Rev. *Sci. Instrum.* **63** 4901

[5] Eldon D *et al* 2012 *Rev. Sci. Instrum* **83** 10E343

[6] Porter GD, Moller J, Brown M and Lasnier C 1998 *Phys. Plasmas* **5** 1410

[7] Stangeby PC 2000 "The plasma boundary of magnetic fusion devices", Institute of Physics Publishing, Bristol

[8] R. Balescu, see Mynick HE, "The generalized Balescu-Lenard collision operator," 1988 Journal of Plasma Physics **39** 303

[9] Eich T *et al* 2011 *Phys. Rev. Lett.* **107** 215001

[10] Makowski MA *et al* 2012 *Phys. Plasmas* **19** 056122

11. Acknowledgments

This material is based upon work supported by the U.S. Department of Energy, Office of Science, Office of Fusion Energy Sciences, using the DIII-D National Fusion Facility, a DOE Office of Science user facility, under Awards DE-AC05-06OR23100, DE-AC52-07NA27344, DE-FC02-04ER54698, DE-FG02-07ER54917 and DE-AC04-94AL85000. DIII-D data shown in this paper can be obtained in digital format by following the links at https://fusion.gat.com/global/D3D.

Appendix A: Some further aspects of the Eich formulation of the target power flux density

The relation between $q_{\|0}$ and $q_{\|\text{-ir-peak}}$ is of interest. We illustrate for the example of $\lambda = w = 5$ mm, from which $\mu = 0.5$, see Fig. A.1, where $s_0 = 0$ has been assumed.

$q_{\|}^{\text{Eich-asymp}}(s)$ is obtained from $q_{\|}^{\text{Eich}}(s)$ by noting that $\lim_{\sigma\to\infty} \text{erfc}(\mu - \sigma) = 2$, thus

$$q_{\|}^{\text{Eich-asymp}}(\sigma) = q_{\|0} e^{\mu^2 - 2\mu\sigma} \quad . \tag{A1}$$

It should be noted that $q_{\|}^{\text{Eich-asymp}}(\sigma = 0)$ is not quite the same as $q_{\|0}$, which is clearly the "upstream" value that we need to compare with $q_{\|e}^{\text{Spitzer}}(R_{\text{sep}}^{\text{std}})$ and $q_{\|e}^{\text{flux-lim}}(R_{\text{sep}}^{\text{std}})$, since $q_{\|}^{\text{Eich-asymp}}(\sigma = 0)$ is larger than $q_{\|0}$ by the factor e^{μ^2} [Fig. A.1(a)]. It is also readily shown that $q_{\|}^{\text{Eich-asymp}}(\sigma = 0)$ is too large to give power conservation: while $\int_{s=-\infty}^{s=\infty} q_{\|}^{\text{Eich}}(s)ds = \int_{s=-\infty}^{s=\infty} q_{\|0} e^{-s/\lambda} ds = q_{\|0}\lambda$, by contrast $\int_{s=-\infty}^{s=\infty} q_{\|}^{\text{Eich-asymp}}(s)ds = q_{\|0}\lambda e^{\mu^2}$ which exceeds $q_{\|0}\lambda$.

As an alternative to comparing $q_{\|0}$ with $q_{\|e}^{\text{X}}(R_{\text{sep}}^{\text{std}})$ we may compare $q_{\|\text{-ir-peak}}$ with $q_{\|e}^{\text{X}}(R_{\text{sep}}^{\text{std}} + \Delta R_{\text{ir-peak}})$. We can identify $q_{\|\text{-ir-peak}}$ as $q_{\|}^{\text{Eich}}(\sigma_{\max})$ in the Eich formulation by noting that the peak occurs at $\sigma = \sigma_{\max}$ where $\frac{dq_{\|}^{\text{Eich}}(\sigma)}{d\sigma} = 0$. This is shown,

Makowski [10], to occur for the value of $\sigma_{max}(\mu)$ satisfying the implicit functional relation:

$$\sqrt{\pi}\mu e^{(\mu-\sigma_{max})^2} erfc(\mu-\sigma_{max}) = 1 . \quad \text{(A2)}$$

The relation $\sigma_{max}(\mu)$ is shown in Fig. A.1(b). It is also readily shown that:

$$q_{||}^{Eich}(\sigma_{max}) / q_{||0} = 0.5 e^{\mu^2 - 2\mu\sigma_{max}} erfc(\mu-\sigma_{max}) . \quad \text{(A3)}$$

See figure A.1(c).

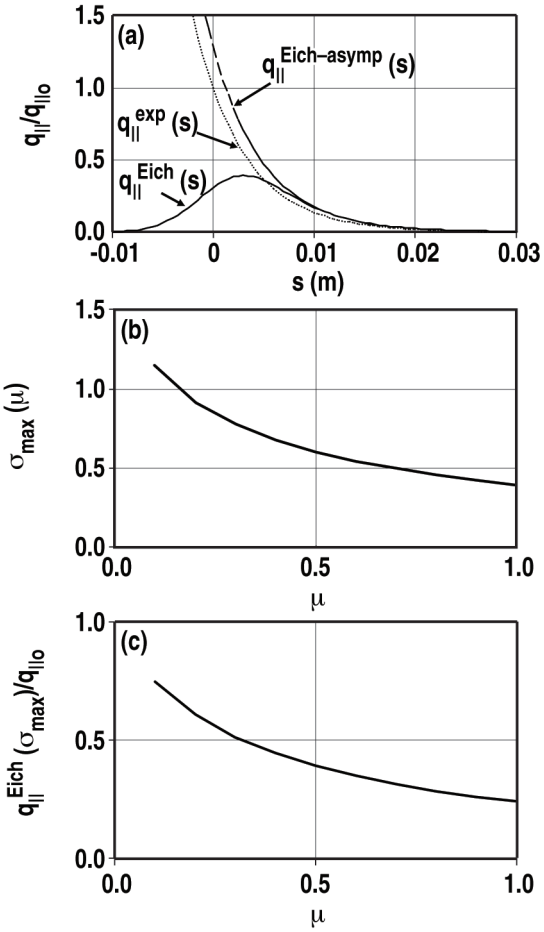

Fig. A.1. Parallel power flux density profiles for the case of = w = 5 mm, thus $\mu = 0.5$, with $s_0 = 0$ assumed. The full Eich expression, $q_{||}^{\mathrm{Eich}}(s)$, equation (9), (solid line). The $s \to \infty$ asymptotic approximation to the Eich expression, $q_{||}^{\mathrm{Eich\text{-}asymp}}(s)$, equation (A.1a) (dashed line). The "upstream" exponential, profile, $q_{||}^{\exp}(s)$, equation (8), (dotted line). (A.1b) The relation $\sigma_{\max}(\mu)$ (A.1c) The ratio $q_{||}^{\mathrm{Eich}}(\sigma_{\max})/q_{||0}$.